Properties of carbon dots versus small molecules from 'bottom-up' synthesis

Zhengyi Bian,^{†,^}Alison Wallum,^{‡,^} Arshad Mehmood,[&] Eric Gomez,[§] Ziwen Wang,[¶] Subhendu Pandit,[¶] Shuming Nie,^{¶,‡} Stephan Link,^{§,°} Benjamin G. Levine,[&] and Martin Gruebele^{‡,^*}

[†]Department of Materials Science and Engineering, [‡]Department of Chemistry, ¶Department of Bioengineering, [‡]Department of Electrical and Computer Engineering, [^]Department of Physics, [^]Center for Biophysics and Quantitative Biology, and [^]Carle-Illinois College of Medicine University of Illinois at Urbana-Champaign, Urbana IL 61801 (USA)

[&]Department of Chemistry and Institute for Advanced Computational Science, Stony Brook University, Stony Brook, NY 11794 (USA)

§Department of Chemistry and °Department of Electrical and Computer Engineering, Rice University, 6100 Main Street, Houston, Texas 77005 (USA)

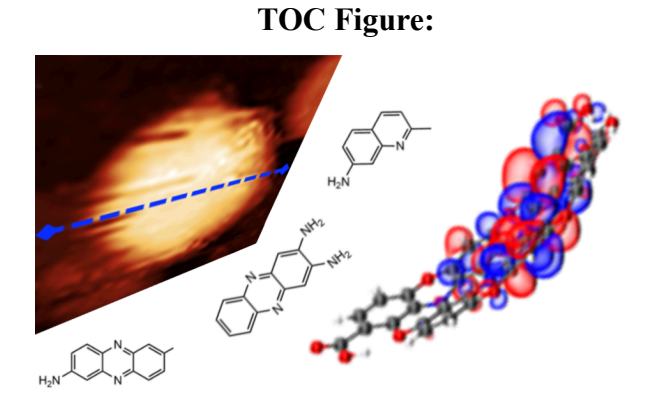
The authors declare no competing financial interest.

[△]Z. B. and A. W. contributed equally to the work.

^{*}Author to whom correspondence should be addressed: Martin Gruebele, orcid.org/0000-0001-9291-8123; email: mgruebel@illinois.edu

Abstract A major challenge in the 'bottom-up' solvothermal synthesis of carbon dots (CDs) is the removal of small molecule by-products, non-carbonized polyamides or other impurities that confound the optical properties. In previously reported benzene diamine-based CDs, the observed fluorescence signal already has been shown to arise from free small molecules, not from nanosized carbonized dots. Here we have unambiguously identified the small molecule species in the synthesis of CDs starting with several isomers of benzene diamine by directly matching their NMR, mass spectrometry, and optical data with commercially available small organic molecules. By combining dialysis and chromatography, we have sufficiently purified the CD reaction mixtures to measure the CD size by TEM and STM, elemental composition, optical absorption and emission, and single particle blinking dynamics. The results can be rationalized by electronic structure calculations on small model CDs. Our results conclusively show that the purified benzene diamine-based CDs do not emit red fluorescence, so the quest for full-spectrum fluorescence from isomers of a single precursor molecule remains open.

Key words: carbon dots, STM, fluorescence, organic fluorophore, fluorescence mechanism



Introduction

Carbon dots (CDs) obtained by 'bottom-up' solvothermal synthesis from small organic molecules, ^{1,2} have garnered much interest because they can be made from affordable precursors, are more biocompatible than semiconductor quantum dots, absorb light strongly, and fluoresce over a range of wavelengths.^{3,4} The general consensus is that such 3-10 nm diameter CDs, when properly carbonized, consist of a core made of polycyclic aromatic hydrocarbons low in hydrogen content and with varying N- and O-content, resulting in bulk or surface fluorophore emission.^{5,6} Single-particle spectroscopy with nanometer spatial resolution has shown that for specific cases^{7,8} the optical absorption by the core is followed by picosecond energy transfer to localized surface sites, where the electronic excitation is quenched by non-radiative intersystem crossing in some CDs, or long-lived enough in other CDs so that it can lead to pH-dependent surface emission with high quantum yield.

A major difficulty in assessing the utility of CDs made by 'bottom-up' synthesis as nano-absorbers and emitters is the presence of small-molecule or polymeric byproducts. These byproducts can mask the emission of CDs. Extensive purification is needed for obtaining proper and valid conclusions. For example, synthesis of CDs¹⁰ can yield a polyamide condensate instead of a carbonized core from citric acid/diamine precursors, and for the same precursors, the fluorescent small molecule byproduct IPCA, when not covalently attached, can obscure nanoparticle fluorescence following insufficient purification. As another example, solvothermal synthesis of CDs from three structural isomers of a single benzene diamine precursor has been reported to result in red, green and blue-fluorescent CDs. However, fast single molecule diffusion of the reaction products revealed that the fluorescence was dominated by small molecules, although an unambiguous identification of the small molecule could not be made. Qu and Sun review the possibility of forming phenazines and polycyclic hydrocarbons the mixture of small molecules and CDs from this solvothermal synthesis.

Here we study the previously proposed¹³ solvothermal synthesis of p-CDs, o-CDs, and m-CDs from para-, ortho- and meta-benzene diamine. We unambiguously identify the small molecules actually responsible for each product fluorescence observed previously,¹³ via mass spectrometry, NMR, optical spectroscopy, and direct matching with commercially available molecular spectra. They are different from the small molecule species suggested previously.¹⁴ We are additionally

able to purify p-, o-, and m- CDs, which are produced in small yields by solvothermal synthesis, and characterize their size, composition, and optical spectra. All three purified CD products fluoresce in the green-blue region, whereas the red fluorescence previously reported for p-CDs comes from phenazine. p- and o-CDs are formed by similar chemistry and have similar optical properties, but m-CDs have a very different chemistry and optical properties. The small molecule fluorophores exhibit mainly two-state blinking in a single molecule microscopy analysis, whereas m-CDs additionally exhibit multi-state blinking as evidence for more than one fluorophore per CD. Computational modeling by time-dependent density functional theory can explain why the p-, o-, and m- CDs differ in their optical properties.

RESULTS AND DISCUSSION

Characterization of small molecule products. We carried out three bottom-up syntheses by subjecting benzene-1,2-diamine, benzene-1,3-diamine, and benzene-1,4-diamine, ('ortho', 'meta' and 'para' isomers) to solvothermal treatment in ethanol at 180 °C for 12 hours, following the methodology of the previously proposed CDs synthesis. ¹³ Fig. 1a illustrates the method and small molecule and CDs products we obtain in the p-, o-, and m-syntheses.

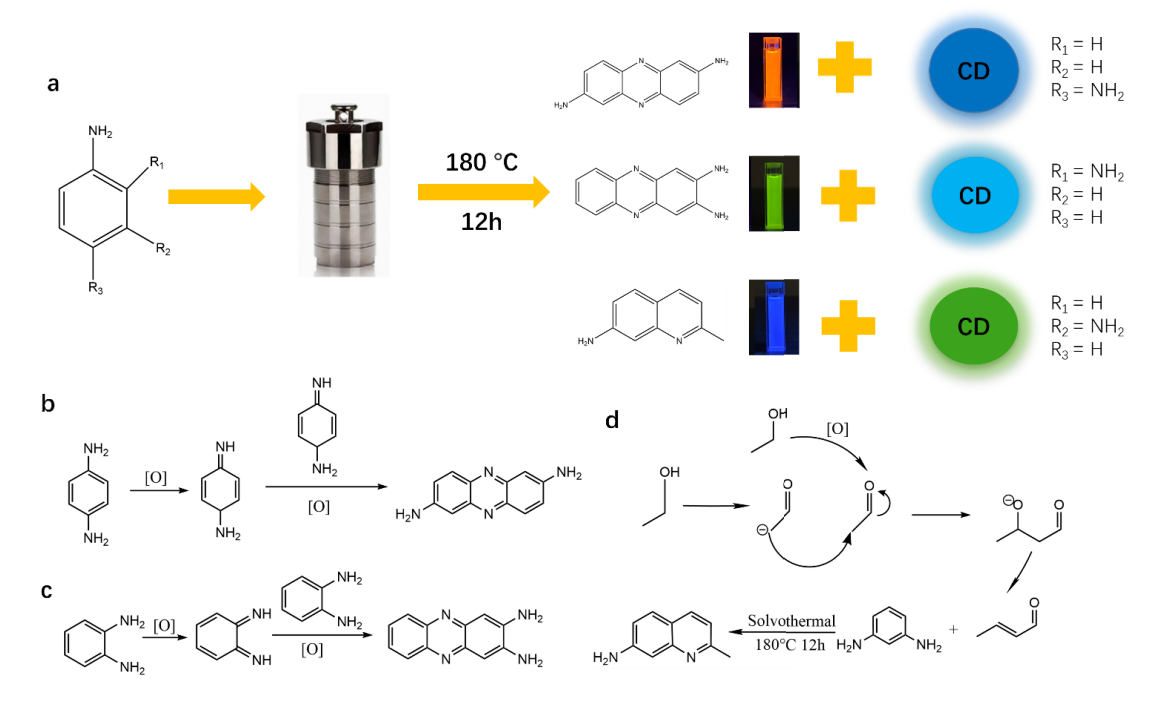


Figure 1. a) Reactions of para-, ortho-, and meta-diaminobenzene to form red, green, and blue, fluorescent small molecules, as well as CDs. b-d) mechanism of formation of 2,7-PDA, 2,3-PDA, and MQA: imine intermediates condense to form phenazine diamines, and crotonaldehyde formed from ethanol in the heated solution reacts with meta-diaminobenzene to make the methylquinoline-amine.

Purification is critical to separate nanoparticles from small molecule condensates formed enroute to the CDs, and a dialysis/column chromatography combination is a proven approach for successful separation. Thus, for purification, the crude product was dialyzed (cut-off 500-1000 Da) against ethanol for 3 days, and both dialysis fractions from inside of the membrane (high mass), and outside of the membrane (low mass) were kept. We focus firstly on the <500 Da outer fraction of small-molecule byproducts. Silica gel chromatography of the fluorescent small molecules from our three solvothermal syntheses yielded three different major by-product phases whose properties were further characterized.

The identity of the dominant small fluorescent molecules that are produced as byproducts during our solvothermal synthesis, and isolated in the low mass dialysis fraction, was determined in several steps. Initially, high-resolution electrospray ionization mass spectrometry revealed that the small molecules produced in both the para- and ortho-reactions yield dominant ions at 211.098 and 212.102 Da (Fig. S1, S3), consistent only with the molecular formula of singly or doubly protonated C₁₂H₁₀N₄, indicating that 2 of the 4 nitrogens are easily protonatable. The major fraction from the meta-reaction has very different peaks at 159.093 and 160.096 Da (Fig. S5), consistent only with a singly- or doubly protonated molecule of formula C₁₀H₁₀N₂.

Two well-known reaction chemistries of benzenes diamine in oxygenated solvents such as ethanol are consistent with these formulas: condensation of o- and p-benzene diamine into diaminophenazines and higher oligomers via quinonoid intermediates^{19–21}, and reaction of m-benzene diamine with crotonaldehyde formed by solvent oxidation to make methylquinoline amines (Fig. 1b-d).²² Table S1 shows all the possible combinations of such products that can form in p-, o- and m-system, although we observed a dominant small molecule product for each reaction by silica gel chromatography of its dialyzed 'outside' fraction.

To identify our small molecule byproducts unambiguously, their ¹H NMR spectra were recorded on a Bruker Avance III 500 MHz spectrometer using deuterated solvent (CD₃OD), and the resulting spectra were compared directly with spectra from commercially obtained molecules or from recrystallized pure reaction product (Figs. S2, S4, S6). The major byproduct from the o-CD reaction matches a commercial sample of phenazine-2,3-diamine, or 2,3-PDA (comm.), with aromatic peaks at 7.96, 7.61, and 7.03 ppm, and an amino proton peak at 4.6 ppm. The major byproduct from the p-CD reaction is the analogous phenzine-2,7-diamine (2,7-PDA), as evidenced by the peaks at 7.77, 7.37, and 7.01 ppm corresponding to protons in the aromatic rings, and the

amino proton peak at 4.60 ppm. The previous assignment of an azo compound's hydrazine nitrogen at 7 ppm¹⁴ to the p-CD reaction product cannot be correct due to instability of the molecule and chemical shift value, although the assignment to a small molecule via fast diffusion is undoubtedly correct. Since 2,7-PDA was not commercially available, we recrystallized pure 2,7-PDA (recryst.) from the low molecular weight byproducts. Finally, the major byproduct from the m-CD reaction is expected not to be a phenazine because the meta position to which the nitrogen directs electrophilic substitution is occupied by another nitrogen (Fig. 1). The small molecule was identified unambiguously again by comparing to a commercial sample as 2-methylquinolin-7-amine (MQA), with ¹H peaks at 8.00, 7.61, and 7.01 ppm corresponding to protons in the aromatic rings, a peak at 4.59 ppm corresponding to a proton in the amino group, and a triplet at 2.62 ppm corresponding to protons in the methyl group. We label the commercially purchased 2-methylquinolin-7-amine as MQA (comm.).

The UV-vis absorbance spectra of the pure molecules (commercial or recrystallized) in ethanol solution in Fig. 2a-c (blue traces) revealed distinct absorption peaks, which were centered at 225 nm, 285 nm, and 510 nm for 2,7-PDA (recryst.); at 205 nm, 260 nm, and 425 nm for 2,3-PDA (comm.); and at 210 nm, 245 nm, and 355 nm for MQA (comm.). Furthermore, the photoluminescence emission spectra of the pure compounds (commercial or recrystallized) in ethanol were recorded upon excitation with light of 365 nm wavelength (red traces in Fig. 2a-c). The maximum emission intensity was observed at 605 nm for 2,7-PDA (recryst.), at 535 nm for 2,3-PDA (comm.), and at 435 nm for MQA (comm.). The time-resolved decay spectra of 2,7-PDA (recryst.), 2,3-PDA (comm.), and MQA (comm.) in Fig. S7 indicates their average lifetime are 8.4 ns, 4. 2 ns, and 1.0 ns respectively, as shown in Table S2.

We next compare the UV-vis absorption spectra of the pure (commercial or recrystallized) small molecules with our low molecular weight dialysis byproducts from the p-, o- and m- hydrothermal syntheses (Fig. 2a-c blue and red dotted traces). Our major small molecule fractions from solvothermal synthesis has absorption and emission spectra nearly identical to commercial samples or literature data,²¹ further supporting the NMR assignment. Similarly, the emission spectra were nearly identical.

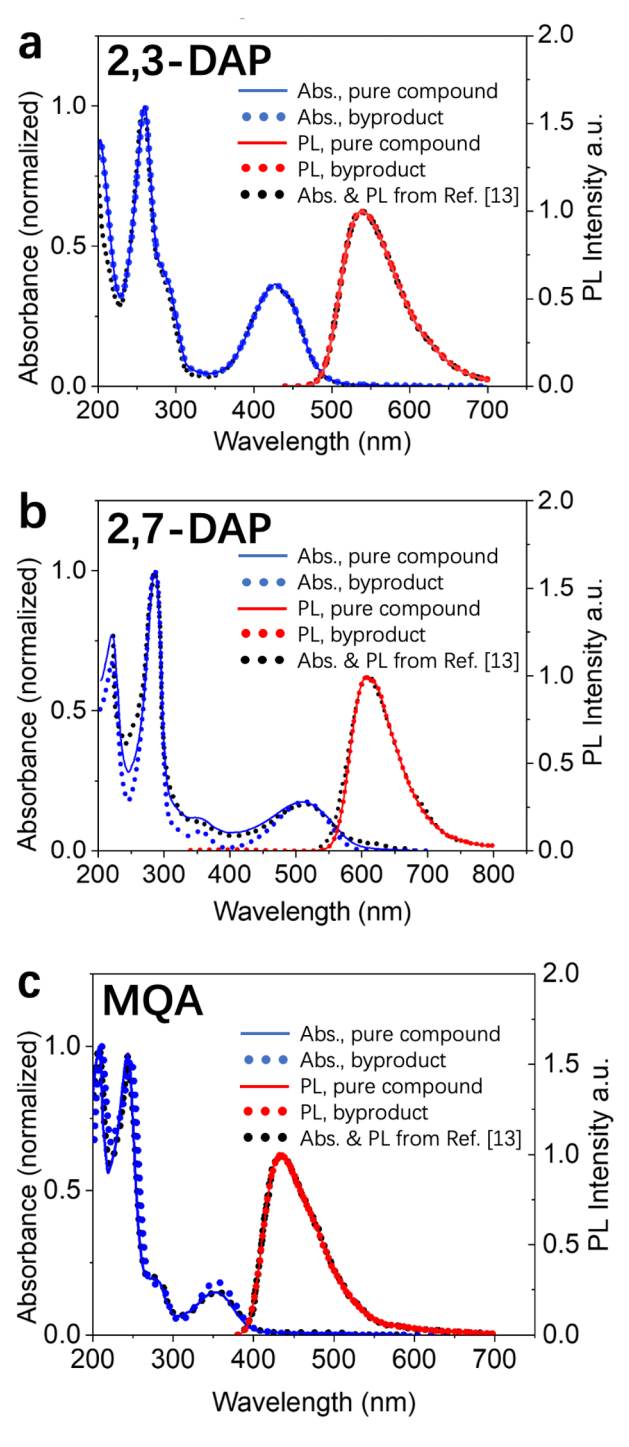


Figure 2. (a-c) UV-vis absorption spectra (Absorbance axis on left) and emission spectra (photoluminescence = PL axis on right) of commercial or recrystallized pure compounds 2,3-DAP (commercial), 2,7-DAP, (recrystallized), and MQA (commercial) shown as solid blue and red curves, compared to the byproducts from our synthesis captured in the low molecular mass (<500 Da) dialysate (dotted blue and red curves), and also compared to the spectra attributed to CDs in ref. [13] (dotted black curves). The 2,3-DAP and MQA spectra match exactly (<2%), while 2,7-DAP shows small differences at low absorbance due to the presence of additional impurities in the raw dialysate (see Table S1). The absorption spectra and emission spectra of our p-, o-, and m- CDs are shown in Fig. 6, and have completely different absorption and emission maxima and shapes.

Finally, we compare both pure molecules, and low molecular weight dialysis byproducts from solvothermal syntheses with the spectra reported previously for the solvothermal synthesis of p-, o-, and m- CDs (Fig. 2a-c black dotted traces). The previously reported spectra are nearly identical to our small molecule byproducts and to the pure compound spectra. The only significant difference is in the low absorbance region of 2,7-DAP, where we attribute to additional byproducts (Table S1) are responsible. Thus we conclude that the absorption and emission spectra in ref. ¹³ belong to the same small molecules that we have identified unambiguously based on commercial or recrystallized samples.

As is typical of small molecules, none of our emission spectra are sensitive to the excitation wavelength, as shown in SI Fig. S8-10. On the other hand, the absorption and emission from our purified carbon dots, discussed in more detail in the next section, is different from any of the small molecules. The purified p- and o-CDs also do not have significant emission when excited at 510 nm for p-CDs and at 420 nm for o-CDs, unlike the assignment reported in ref. ¹³ and seen for our small molecule byproducts in SI Fig. S8-10.

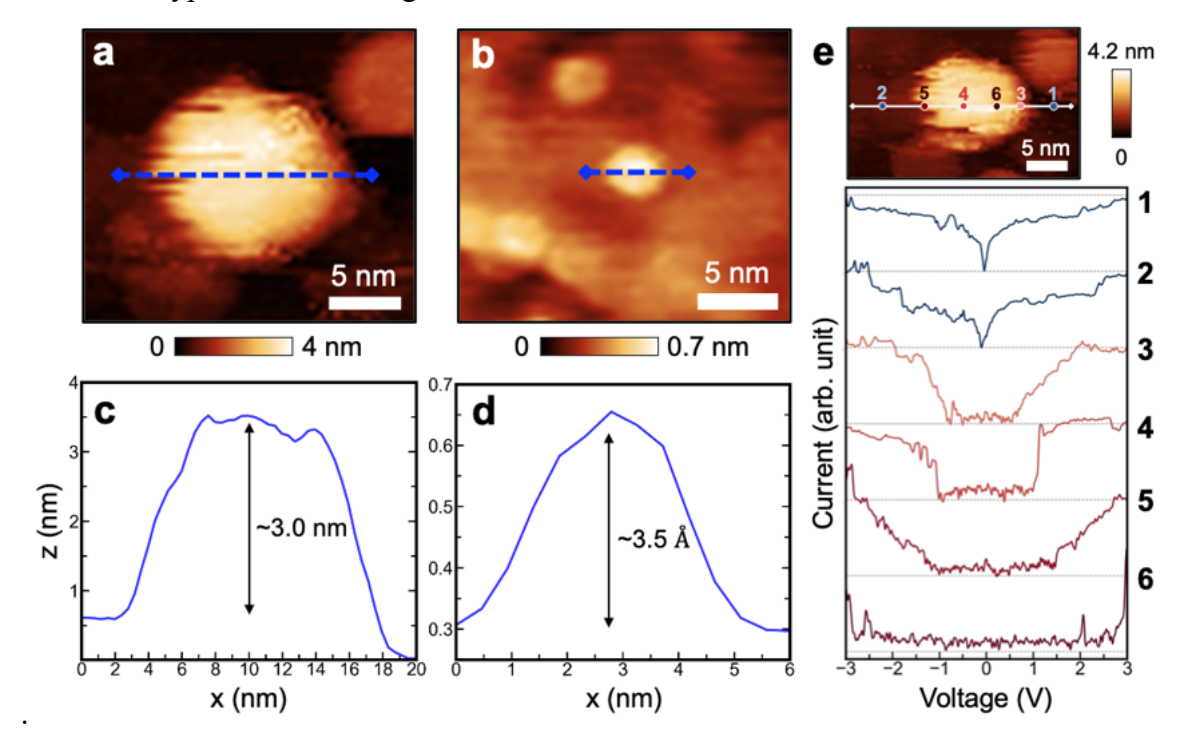


Figure 3. STM of o-CDs and synthetic byproducts. (a, b) STM topography images of two characteristic structures seen in undialyzed o-CD samples. (c, d) Corresponding height profiles along blue dotted lines shown in topography images. We classify structures > 2 nm in height as CDs, while small structures with < 0.5 nm height are classified small molecule reaction byproducts. (e) Scanning tunneling spectroscopy (STS) across an individual dot produced from o-CD synthesis shows bandgaps ranging from semiconducting to insulating. Scanning conditions: 2.0 V, $5 \times 10^{-11} \text{ A}$.

Characterization of carbon dot products. The insufficiently purified samples that were previously reported¹³ are still very likely to contain CDs based on the published TEM data. Our scanning tunneling microscopy (STM) data on the original undialyzed reaction products (Fig. 3) indeed confirms the presence of CDs. Nonetheless, given the prominent populations of small molecules whose spectra are shown in Fig. 2a-c, the distinct spectra corresponding to CDs are likely obscured in undialyzed reaction products. Thus, we further purified the inner high mass fraction (>500 Da) from our dialysis by normal-phase silica gel chromatography. CDs were isolated after this additional chromatographic separation from small molecules, and the presence and size of CDs was confirmed using TEM.

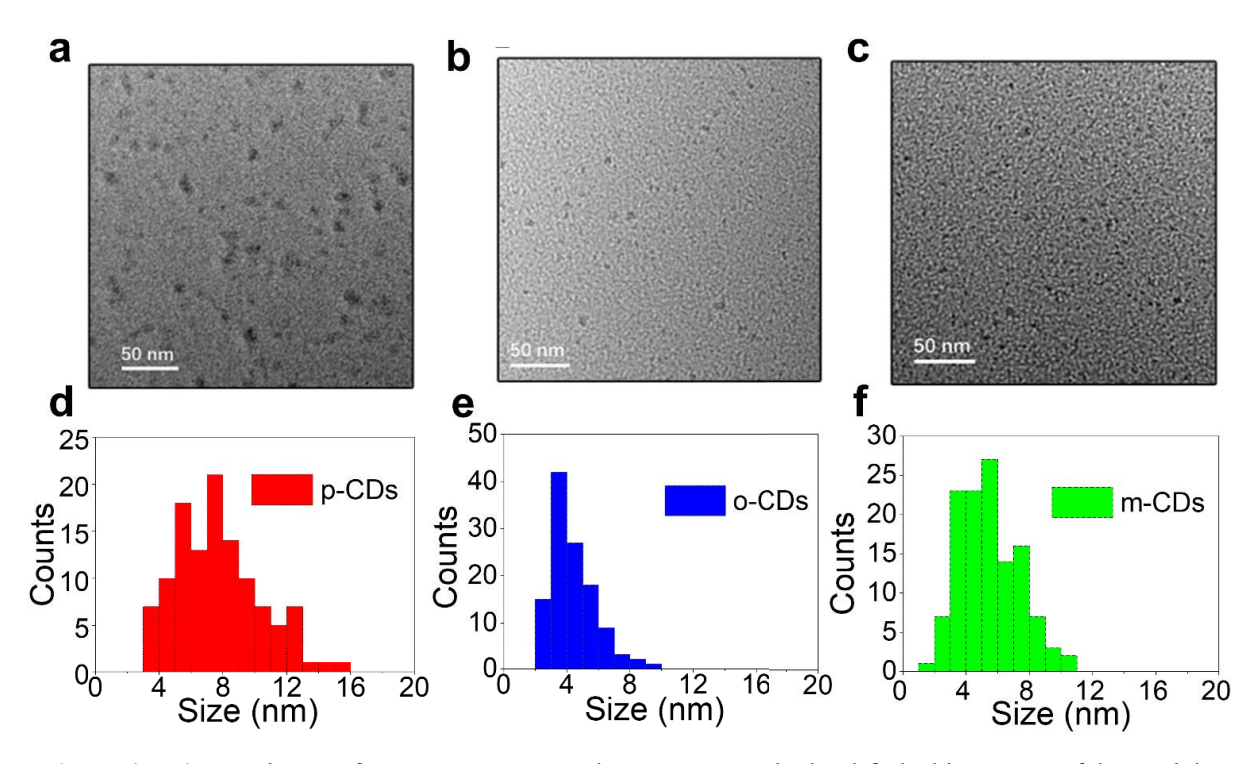


Figure 4. a-c) TEM images for p-CDs, o-CDs, and m-CDs respectively; d-f) the histograms of the particle size distribution of p-CDs, o-CDs, and m-CDs respectively.

For scanning tunneling microscopy (STM) measurements, we deposited the o-CD reaction products subjected only to a column purification on a gold surface by aerosol deposition. We expect this mixture to contain both CDs and small molecule byproducts that should be visible by STM imaging. Fig. 3a,c reveals the presence of larger carbon dots among a large excess of small molecules and polycyclic aromatic hydrocarbon byproducts (Fig. 3b,d). Particles of height < 0.5 nm that we classify as small molecules were at least 10 times more abundant than particles of > 2 nm height that we classify as CDs. This observation is consistent with small molecule spectra

obscuring the CD spectra. STM reveals that the CDs can be oblate in shape, an indication that they could be growing via layering of large polycyclic aromatic hydrocarbons formed from the small molecules such as phenazines and quinoline amines. The I-V curves at various locations on or near a carbon dot in Fig. 3e confirm the detection of the metallic gold surface (traces 1 and 2), and reveal dots with local bandgaps in the \sim 2-6 eV range (traces 3 – 6), consistent with the possibility of absorption as blue as \sim 200 nm and emission as red as 600 nm.

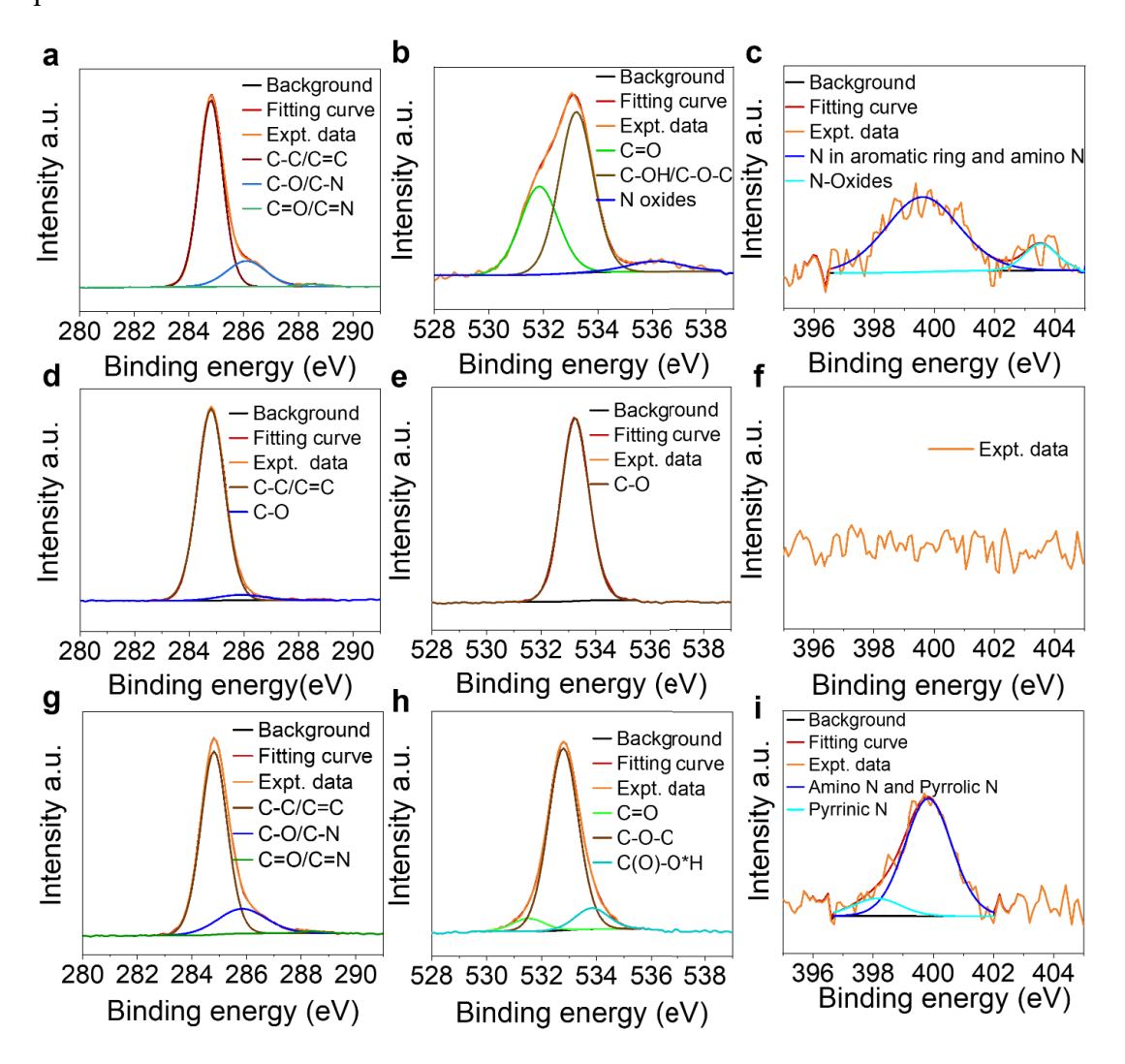


Figure 5. High resolution XPS C 1s, O 1s and N 1s spectra of (a-c) p-CD, (d-f) o-CDs, and (g-i) m-CDs. Elemental compositions are shown in Table S2. The near-surface nitrogen content was low in the p- and o-CDs, consistent with the highly simplified model structures for calculations in Fig. 8.

We used transmission electron microscopy (TEM) to investigate the particle size distributions of p-, o-and m-CDs from the inner dialysis solution purified further by silica column chromatography. As shown in Fig. 4a-c, we do obtain CDs from p-phenylenediamine, o-

phenylenediamine, and m-phenylenediamine. p-CDs have an average diameter of 8.1 nm, while o-CDs have an average diameter of 4.3 nm, and m-CDs have an average diameter of 5.4 nm, with size histograms in Fig. 4d-f. The morphology of the particles projected in 2D generally had an aspect ratio less than 2:1. Using high-resolution cryo-TEM, we find that the particles are amorphous and do not show diffraction associated with graphenic layers. This is supported by the comparison in SI Fig. S11 between our bottom-up CDs and a control sample of crystalline top-down CDs synthesized from graphite powder.

X-ray photoelectron spectroscopy (XPS) was used to analyze the surface composition and oxidation of p-, o-, and m-CDs. A detailed summary, survey spectra (Fig. S12-14), and elemental composition (Table S3) are provided in the SI. As can be seen in Fig. 5, the spectra show a combination of sp²/sp³ hybridized carbon. All three types of CDs show evidence for strong surface oxidation due to the oxygenated solvent (ethanol) used in the high temperature synthesis. By comparison, the CDs' surfaces are depleted in nitrogen, with p-CDs showing some evidence of N-oxides, o-CDs showing no detectable surface nitrogen, and m-CDs showing the largest fraction of surface nitrogen. Despite the nitrogenous small molecule reactants, solvothermal synthesis of CDs in ethanol produces dots consistent with a high C=O (e.g. carboxylate) and C-O (e.g. hydroxyl) content at the surface, which likely leads to pH-sensitive emission.

In order to characterize the optical properties of the p-, o-, and m-CDs, we performed UV-vis absorption and fluorescence measurements. Fig. 6a-c shows that the absorption and emission spectra of the p-, o-, and m-CDs are distinct from the small molecules in Fig. 2a-c. In particular, the p- and o-CD emission is blue shifted from the small molecule byproducts, whereas the m-CD fluorescence is red-shifted, indicating that the fluorophore of m-CDs is different from that of p- and o-CDs. Unlike the proposal in ref. ¹³, none of the p-, o-, and m-CDs have red fluorescence (Fig. 1a and 6a-c).

The fluorescence spectra also were recorded as a function of excitation wavelength as shown in Fig. 6. The emission of p- and o-CDs is only weakly excitation wavelength-dependent, but increases at longer excitation wavelengths even though the absorption cross section decreases, indicative of enhanced quantum yield. The emission of m-CDs has a highly wavelength-dependent peak, indicating the existence of more than one emissive site and at least one additional fluorophore on m-CDs, not present on p- or o-CDs. The decay curve of p-, o-, and m-CDs in Fig. S15 indicates the average fluorescence lifetime are 1.3 ns, 2.3 ns, and 3.3 ns respectively, as shown in Table S4.

Unlike the small molecules (SI Figs. S8-10) and the assignment from ref. ¹³, the purified o-CDs and p-CDs do not show significant fluorescence when excited at longer wavelengths (420 or 510 nm) (SI Figs. S16-17).

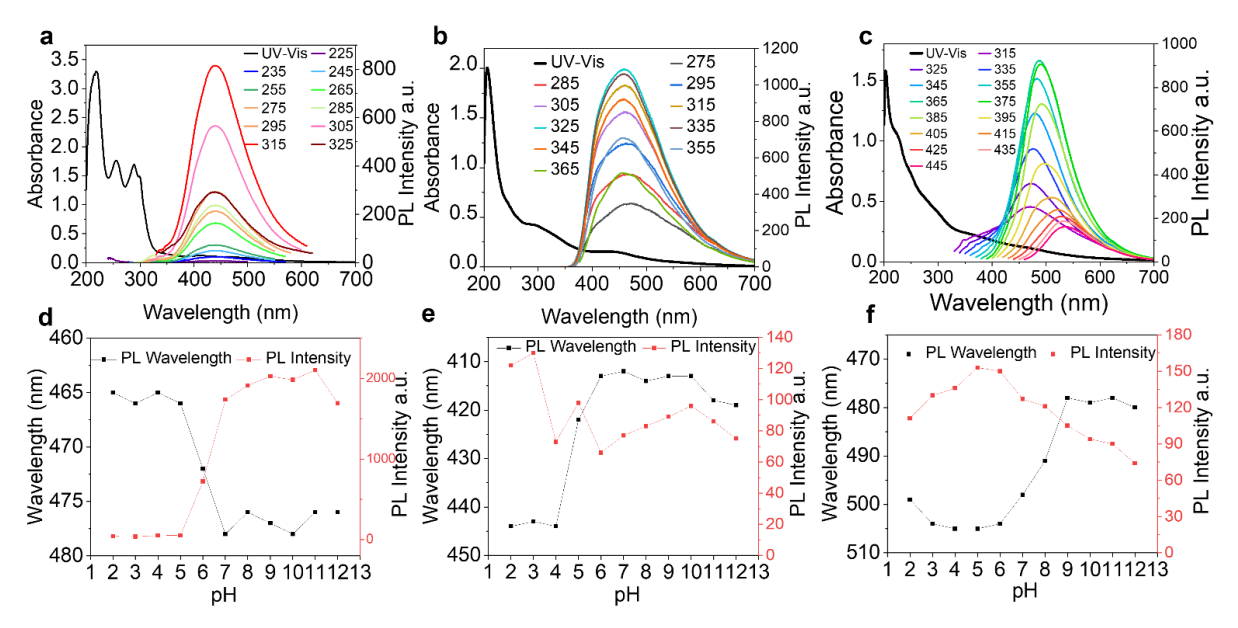


Figure 6. a-c) UV/Vis absorption spectra (black traces) and PL emission spectra (color traces) of p-CDs, o-CDs, and m-CDs in ethanol solution. d-f) Variation of maximum emission wavelength and intensities of p-, o-, and m-CDs as a function of pH. Photoluminescence (PL) error bars are one standard deviation of the mean from repeat measurements.

We observe pH-sensitive absorption and emission properties for all three CDs in agreement with the surface functional groups we expect to see from our XPS data. These surface functional groups are solvent-exposed and can ionize, affecting their electronic structure and fluorescence properties. The pH sensitivity shown in Fig. 6 reveals that all three dots have different fluorophores. For the p-CDs, reduced fluorescence is observed below pH 7, consistent with protonation of a phenolic hydroxyl group (pKa 7-9) in the fluorophore. For the o-CDs, fluorescence increases by a factor of 2 upon protonation below pH 4, consistent with a carboxylate group (pKa 4-5) that changes the environment near the fluorophore when protonated: the protonation of the carboxylate group can lead to a decrease in the internal charge transfer (ICT) process within the carbon dots, resulting in an increase in fluorescence intensity. m-CDs have a bimodal behavior with maximum fluorescence at pH 5, consistent with at least two fluorophores containing different pKa groups present, and thus consistent with the more complex emission in Fig. 6c. Singular value decomposition analysis in Fig. S18 was conducted on the PL spectrum of the m-CDs. We find that there are 3 major singular values present in the emission spectra of the m-CDs, consistent with the

excitation wavelength-dependence and the more complex pH-dependence in Fig. 6 and more than a single dominant chromophore at the surface of the m-CDs.

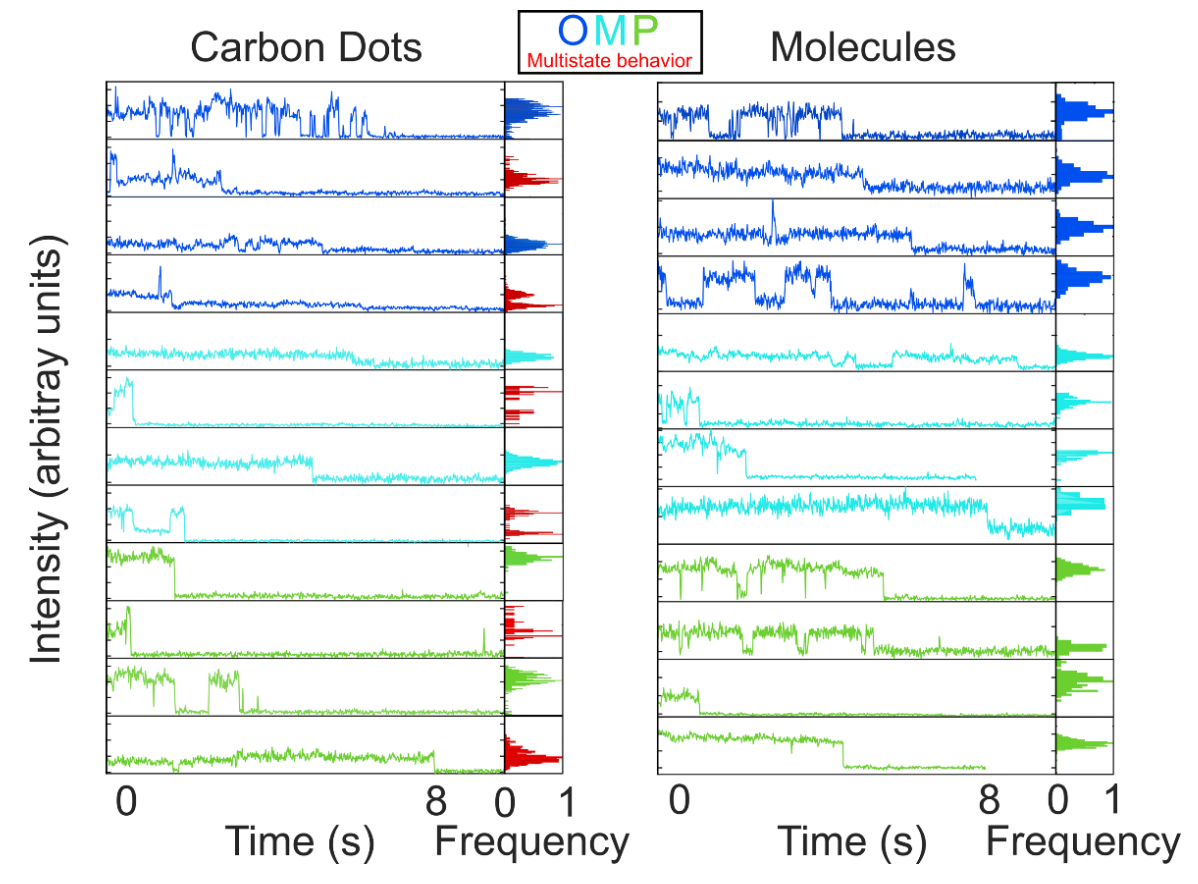


Figure 7. Unpolarized single particle fluorescence of o-, m-, and p- CDs (left) and the corresponding phenazines and quinoline-amine (right): 2,3-PDA (dark blue), MQA (cyan), 2,7-PDA (green). The small molecules have blinking largely consistent with two-state behavior, whereas some CDs have more complex emission time series, including multiple distinct emission levels for two of the m-CDs and one each of the p- and o-CDs. To the right of the trajectories, corresponding intensity histograms are shown, with those colored red referring to CDs with clear multistate behavior.

To follow up on the complex emission properties of CDs, single-particle fluorescence imaging experiments shown in Fig. 7 reveal distinct blinking characteristics across small molecule and CD p-, o-, and m- reaction products (see SI Fig. S19 for multi-state analysis). Small molecules such as phenazines and quinoline amines are more likely to show two-state behavior during blinking. 2,7-PDA and MQA show two-state behavior, while 2,3-PDA shows some evidence for a third state. The CDs, and in particular the m-CD, in several cases show multi-state blinking with well-separated intensity levels for different states, which we assign to the presence of multiple surface fluorophores. The three or more distinct fluorescence intensity levels seen for m-CDs is consistent with their excitation wavelength-sensitive and pH-sensitive emission spectra in Fig. 6, as well as

multiple distinct components in the fluorescence spectrum as a function of excitation wavelength (SI Fig. S18), indicative of at least two pH-sensitive fluorophores.

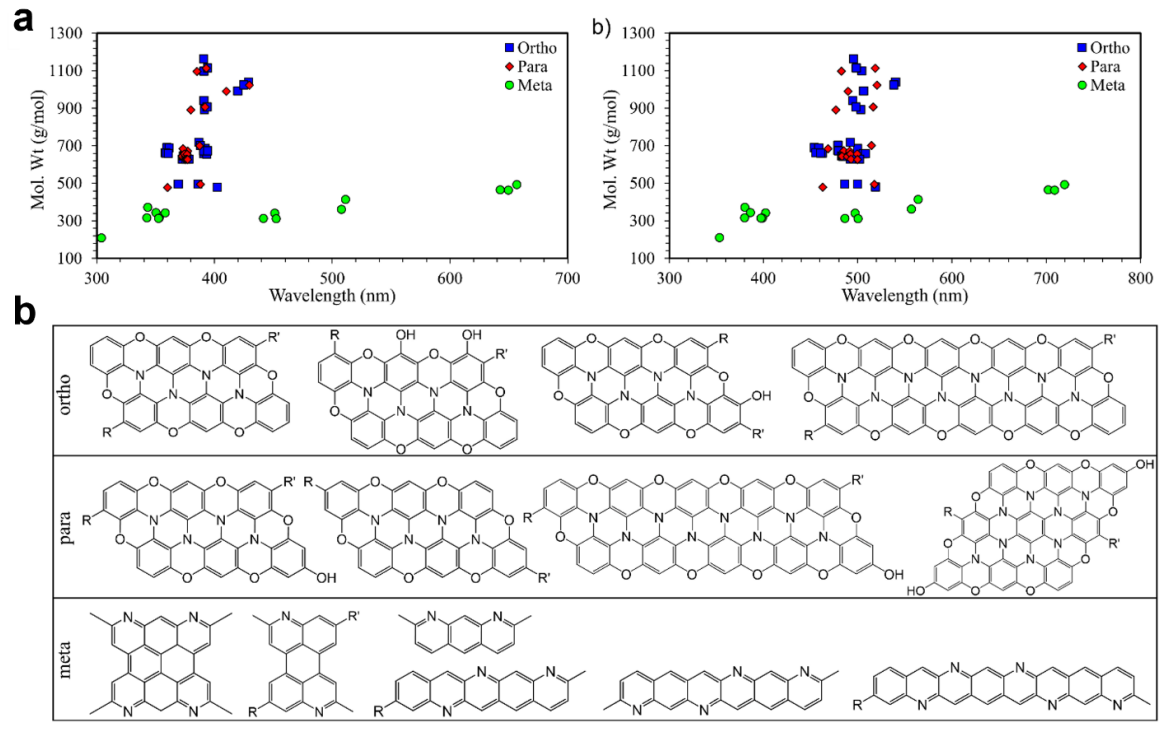


Figure 8. Absorbance (a) and emission (b) energies of model CDs calculated at the CAM-B3LYP/6-31G(d,p) level, decorated with carboxyl, hydroxyl, and amine groups. (c) Representative structures of the o-, p- and m-CD highly simplified single-layer models used in the calculations. The absorbance and emission plots include models of o- and p-CDs ranging from 9 to 27 cyclic rings.

Computational spectroscopy of model carbon dots. To understand how atomistic structure determines the different emission properties of the p-/o- vs. m-CDs, linear response time-dependent density functional theory^{23–29} (TDDFT) was applied to plausible but highly simplified simulation model structures based on phenazine vs. quinoline amine (Fig. 8). Single layer model structures for o- and p-CDs were generated by assembling 2,3-PDA and 2,7-PDA units, respectively. Structures for m-CDs were generated by assembling MQA units, sometimes with additional crotonaldehyde units. Consistent with the XPS data above, which is sensitive to surface elements, -NH₂ groups were oxidized in many cases, therefore, surface -R and -R' groups are mainly -O-, -OH, or even -COOH groups, explaining why p-CDs and o-CDs are depleted in surface nitrogen in Fig. 5c and 5f: they contain mostly internal sp³-hybridized nitrogen. Also consistent with the larger XPS nitrogen signal in Fig. 5i for m-CDs, the m-CD models in Fig. 8 have many exterior sp² hybridized nitrogens.

Fig. 8a,b shows the distribution of calculated vertical excitation and emission energies for a set

of single-layer structures with various molecular weights. Representative structures are presented in panel c while the complete list and labels are given in Table S5-7. A comparison of the models shows that the m-CDs have a much wider range of vertical excitation and emission energies relative to the p- and o-CDs, even though a wide range of molecular weights are explored in the p- and o- cases. The wide range of emission energies is consistent with the experimental observation of strong excitation wavelength dependence in the emission spectrum of the m-CDs (Fig. 6). In the model o- and p-CDs, sp³ nitrogen centers disrupt conjugation, resulting in size-insensitivity of the absorption and emission energies. The absence of sp³ nitrogen centers enables more extended conjugation in the model m-CDs (Figs. S21-26). Different surface R groups are predicted to shift the gaps only slightly—e.g., the emission energies of hydroxylated CDs are only ~20 nm blue-shifted relative to structurally similar carboxylated species. Thus surface modification modulates, but is not the primary controlling factor, of emission wavelength in our model calculations.

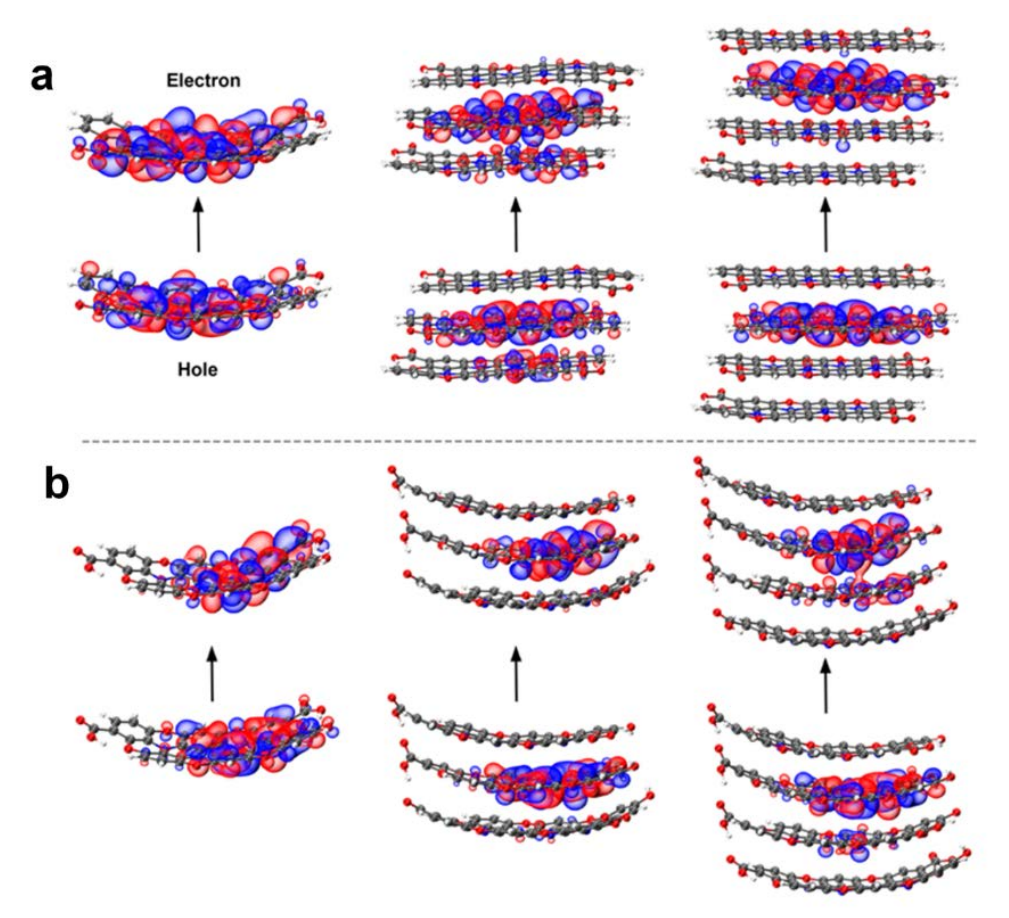


Figure 9. Effect of the number of layers on the electron (top) and hole (bottom) orbitals of models of (a) o-CDs and (b) p-CDs. Systems with one, three, and four graphitic layers are shown from left to right. The electron and hole are shown as natural transition orbitals, plotted using the VMD software package.³⁰

To further investigate the degree of delocalization of excitations in CDs, we computed several o- and p-CDs, with one, three, and four layers. The orbitals corresponding to electron and hole are presented in Fig. 9. The sp³ N atoms induce curvature in several of the structures, and this could be a reason for the more amorphous structure of CDs containing non-aromatic nitrogen (or oxygen) atoms in the core. In the three-layer models, the transitions involve the central layer with negligible contribution from the outer layers. In the 4-layer models, the outermost layers also do not contribute to the excitation, and only weak delocalization is observed between the internal layers. The excitation energies of the 4-layer systems therefore are red-shifted by only 20-30 nm relative to the 3-layer systems, consistent with minimal interlayer delocalization (Fig. S19). The same trends are observed in additional o- and p- models (Figs. S20 and S21).

To examine the impact of the solvation on the vertical excitation and de-excitation energies, we conducted the geometry optimizations of the selected systems of carboxyl substituted p-, o-, and m- CDs. This optimization was carried out using the equilibrium linear response polarizable continuum solvation model (LR-PCM) at the same level of theory. Subsequently, the excitation and de-excitation energies were calculated using the non-equilibrium LR-PCM method, and the results are presented in Fig. S27. The analysis revealed that, on average, the excitation energies experienced a redshift of 20 nm when compared to the gas phase energies. The minimum redshift observed was 4.4 nm for the O1 model, whereas the M5 model exhibited the maximum redshift of 38.1 nm. Likewise, the vertical de-excitation energies also displayed a redshift, averaging around 26 nm. However, the calculated absorbance and emission energies in solvent obey the same trends as observed in the gas phase, thus the conclusions of the simulation work in this paper are robust to solvation environment.

Conclusion Carbon dots are intrinsically emissive carbonized materials in the nanometer size range with some heteroatom content and low hydrogen content. Many precursors have been proposed for bottom-up synthesis of CDs, ^{13,14} and these precursors can produce a variety of byproducts in addition to carbon dots. However, studies including methods such as NMR analysis and diffusion measurements have shown that in some bottom-up products, traditional carbon dots may not be the primary contributor to bulk optical properties. This can result from 'carbon dots' that are not carbonized, but rather an aggregate of oligomeric polymers such as polyamides, ¹¹ or that the fluorescence attributed to CDs that comes from small molecule byproducts that may be

free or only loosely attached to the dot.^{12,14,31,32} Here we unveiled the specific small molecules responsible for red-green-blue fluorescence previously attributed to CDs synthesized from three structural isomers of diaminobenzene. The molecules are unambiguously identified via comparison of mass, NMR, absorption, and emission spectra. The molecules are of interest because further oxidation and condensation reactions of the type shown in Fig. 1 presumably eventually build up the core of the CDs, as shown in the hypothetical single layer structures in Fig. 8.

Fortunately, it is possible to obtain CDs of relatively uniform size distribution from the solvothermal processing of benzene diamines, as can be seen from the TEM data in Refs. ^{13,14} and in Figs. 3 and 4 here. These dots, after careful combined dialysis and column purification, have characteristic fluorescence, but with absorption and emission peaks quite different from the small molecules. Unfortunately, all three CD species fluoresce in the blue and green region of the spectrum, with the m-CD (not the p-CD, as previously thought) the most red-shifted due to its significantly different synthesis pathway and composition.

The composition and properties of all three CDs differ substantially, highlighting that different isomers can lead to different chemistry. In particular, the m-CD differs substantially from the p-and o-CDs because its meta position, to which electrophilic reactivity would normally be directed, is occupied by an amino group: the m-CD likely lacks sp³ hybridized nitrogen centers, making its emission range much broader due to more extensive conjugation. m-CD emission is red-shifted compared to its small molecule precursors, and its fluorescence spectrum shows a more complex excitation wavelength-dependence indicative of multiple fluorophores (possibly both bulk and surface fluorescence in the visible wavelength range). This is corroborated by the non-monotonic pH dependence of the fluorescence, more complex blinking behavior than any of the other dots or small molecules, and TDDFT calculations. Our analysis shows that, by varying isomers of the same precursor, it is possible to make CDs that predominantly have only one fluorophore (p and o) as well as CDs that have multiple fluorophores (m).

The task of producing three-color RGB CDs from isomers of a single precursor with bottomup syntheses thus must be revisited. This work and other recent work discussed above highlight the need for rigorous purification and characterization of carbon dot syntheses products. It is likely that one will discover other cases where the observed emission can be attributed to small molecules unattached to carbon dots, or where the nanomaterial is a polymer obtained from multi-functional precursors (diacids, diamines, or diesters) rather than a carbonized material of the type expected from top-down synthesis, with a high absorption cross section and efficient energy transfer from core to surface fluorophores.⁸

Experimental Methods

Materials

Methanol, Ethanol (200 proof), p-phenylenediamine (>98%, Sigma-Aldrich), o-phenylenediamine (99.5%, Sigma-Aldrich), m-phenylenediamine (99%, Sigma-Aldrich), Dichloromethane, Ethyl Acetate, Dialysis Tube (MWCO 500-1000Da, cellulose ester membrane), phenazine-2,3-diamine (Sigma-Aldrich), MQA(>98%, Ambeed Inc.), All chemical reagents were used as received, without further purification. Phenazine-2,7-diamine was not commercially available. We recrystallized the product of solvothermal synthesis from solution after addition of water and cooling to 4 °C to reduce solubility. Dark red crystals of 2,7-PDA were obtained.

Synthesis of p-CDs, o-CDs, and m-CDs and small molecules

CDs were synthesized via a one-pot solvothermal route following a previously reported method in Ref.¹³ with some modifications in purification. To synthesize p-CDs and phenazine-2,7-diamine, 0.90 g of p-phenylenediamine was dissolved in 90 ml ethanol, and the solution was sonicated for 1 min to obtain a clear solution. The solution was then transferred to a 100 ml PTFE liner, which was placed in an autoclave and heated at 180 °C for 12 hours. After cooling to room temperature, the resulting raw product was transferred to a dialysis tube with a molecular weight cutoff (MWCO) of 500-1000 Da and dialyzed against ethanol as a buffer for 72 hours, with the buffer being changed every 24 hours. To collect the p-CDs and phenazine-2,7-diamine separately, the dialysis tube was removed, and the solution was divided into inside and outside solutions. Silica gel chromatography was used to purify the mixture, with the eluent consisting of a mixture of dichloromethane and methanol. For the purification of the CDs, eluents with pure ethyl acetate were used to remove most impurities, and the p-CDs were collected. Sephadex G-25 Medium SEC column with 20% ethanol as eluent can also be used for high purity p-CDs after the dialysis as another optional purification method. To purify the crude phenazine-2,7-diamine, eluents with pure ethyl acetate were used to obtain phenazine-2,7-diamine with high purity in silica gel chromatography.

For o-CDs and 2,3-diaminophenzaine, o-Phenylenediamine (0.90 g) was dissolved in 90 mL of ethanol and sonicated for 1 min to obtain a clear solution. The solution was then transferred to a 100 mL liner, placed in an autoclave, and heated at 180 °C for 12 h. After cooling to room temperature, the resulting product was transferred to a dialysis tube with a molecular weight cutoff (MWCO) of 500-1000 Da and dialyzed against ethanol as buffer for 72 hours, with buffer replacement every 24 hours. The dialysis process yielded separate solutions of o-CDs and phenazine-2,3-diamine, which were collected from inside and outside the dialysis tube, respectively. Silica gel chromatography was used for further purification, with DCM:methanol (99:1) as the initial eluent to remove impurities from the CDs. The purified CDs were collected using a second eluent, DCM:methanol (95:5). To purify the crude phenazine-2,3-diamine, pure ethyl acetate was used as an eluent in the silica gel column. The purified phenazine-2,3-diamine was collected after passing the column with the eluent.

For m-CDs and 2-Methylquinolin-7-amine,0.90 g of m-phenylenediamine was dissolved in 90 mL of ethanol and sonicated for 1 minute to obtain a clear solution. The solution was then transferred to a 100 mL liner and heated at 180 °C for 12 hours in an autoclave. After cooling to room temperature, the raw product was transferred to a dialysis tube with a molecular weight cutoff (MWCO) of 500-1000 Da and dialyzed against ethanol for 72 hours, with the ethanol buffer being changed every 24 hours. m-CDs and 2-Methylquinolin-7-amine were collected separately from inside and outside solutions after dialysis. To purify the m-CDs and 2-Methylquinolin-7-amine, silica gel chromatography was performed using a mixture of dichloromethane (DCM) and methanol as eluent. For purification of the CDs, the eluent with a 10:90 ratio of methanol to DCM was used initially to remove most impurities, followed by a new eluent with a 40:60 ratio of methanol to DCM to collect the CDs. For purification of the crude 2-Methylquinolin-7-amine, the eluent with a 4:96 ratio of methanol to DCM to obtain 2-Methylquinolin-7-amine with high purity in silica gel chromatography.

Instruments and Characterization

Transmission electron microscopy. The morphology of the CDs was characterized using a transmission electron microscope (JEOL 2100 cryo TEM) operating at an accelerating voltage of 120 kV. To prepare the samples, they were drop-cast onto ultrathin carbon-coated copper grids and then dried in air.

NMR spectroscopy. For ¹H nuclear magnetic resonance (NMR) spectroscopy, CD samples were dissolved in CD3OD solutions and analyzed at 25 °C on a Bruker AV500 spectrometer at a ¹H NMR operating frequency of 500 MHz. The solvent signal was used as an internal standard to reference the spectra.

UV-Visible absorbance and photoluminescence measurements. The absorption spectra were recorded in the 200-700nm range using a GENESYS 10S (Thermo Scientific) UV-Vis spectrophotometer. Fluorescence measurements were made using a Shimadzu RF-6000 spectrofluorometer, with the fluorescence lifetimes measured by time-correlated single-photon counting (TCSPC) using a CHIMERA spectrometer (Light Conversion) with an excitation wavelength of 400 nm. The fluorescence decay curves were analyzed with SPCImage fitting program to calculate the lifetime. All spectra were measured at room temperature using a 10 mm path-length quartz cuvette.

X-ray photoelectron spectroscopy. X-ray photoelectron spectroscopy (XPS) measurements of the CDs were performed on a thick, vacuum-dried layer of the samples applied to a glass surface using a Physical Electronics PHI 5400 spectrometer with Al Kα (1486.6 eV) radiation. The spectra were referenced to the adventitious C 1s feature at 284.8 eV. CasaXPS was used for analysis of the XPS data, with the standard error of peak area quantification being less than 5%.

Blinking measurements. Single molecule fluorescence imaging was performed on a home-built sample scanning confocal microscope consisting of an inverted microscope (Zeiss), 488 nm diode laser (Coherent), a piezo scanning stage (Physik Instrumente), and an avalanche photodiode (APD) detector (Perkin Elmer). Samples were immobilized on glass coverslips by spin-coating, and individual molecules or particles were initially identified by creating a fluorescence image. The sample stage was then positioned so that a single object was excited in the confocal excitation spot, and the emission, filtered by dichroic and long pass filters, was continuously detected until photobleaching by the APD, connected to a counter board (Becker & Hickl) with an integration time of 10 ms.

Scanning tunneling microscopy measurements. Scanning tunneling microscopy experiments were performed on a home-built ultrahigh-vacuum (UHV) STM. All experiments were done under UHV (base pressure ~1E-10 torr) at room temperature. Samples were prepared on Au(111) films on mica (Phasis) which are UV-ozone treated, H₂ flame annealed, and then mounted in an STM sample carrier with tantalum foil contacts. Each Au(111) substrate was degassed for 12 hours and imaged via STM prior to sample deposition. Following substrate imaging, undialyzed o-CD samples were then deposited via pulsed aerosol deposition (Iwata CM-SB airbrush) using N₂ as a carrier gas. Samples were then re-loaded into the STM, degassed via filament heating at <35 °C for ~1-3 hrs, and outgassed for 24+ hrs. Topography and spectroscopy measurements were collected with Ir coated W tips (TipTek) with scanning currents ranging from 5 – 100 pA. All tips used were degassed via resistive heating for 12+ hours prior to use.

ASSOCIATED CONTENT

SI Supporting Information

The Supporting Information is available free of charge at https://pubs.acs.org/doi/10.1021/acsnano.XXXXX.

Tables of small molecule byproducts, extended results NMR, mass, and optical spectra, TEM comparison of amorphous and crystalline (top-down) carbon dots, more XPS and blinking data, and computational methods are available in the supplementary information PDF.

Acknowledgement

This work was supported by a CCI grant from the National Science Foundation, the Center for Adopting Flaws as Features, CHE-2124983. ZB acknowledges training and help with sample preparation by Dr. Indrajit Srivastava, and we thank Dr. Srivastava for pointing us to the p-, o-, and m- CDs as an interesting area for study. MG acknowledges support by the James R. Eiszner Chair. AM and BGL gratefully acknowledge funding from the Institute for Advanced Computational Science. S.L thanks the Robert A. Welch Foundation for support through the Charles W. Duncan, Jr.-Welch Chair in Chemistry. We also thank Dr. Xiuli Mao's help in Mass Spectroscopy characterization, Dr. Richard Hasch from the Materials Research Lab for his assistance with XPS measurements Dr. Kristen M Flatt for the assistance in High-resolution TEM, and Ziwei Wu for help in SVD analysis.

References

- (1) Li, H.; Kang, Z.; Liu, Y.; Lee, S.-T. Carbon Nanodots: Synthesis, Properties and Applications. *J. Mater. Chem.* **2012**, *22* (46), 24230. https://doi.org/10.1039/c2jm34690g.
- (2) Zhang, Y.-Q.; Ma, D.-K.; Zhuang, Y.; Zhang, X.; Chen, W.; Hong, L.-L.; Yan, Q.-X.; Yu, K.; Huang, S.-M. One-Pot Synthesis of N-Doped Carbon Dots with Tunable Luminescence Properties. *J. Mater. Chem.* **2012**, *22* (33), 16714. https://doi.org/10.1039/c2jm32973e.
- (3) Srivastava, I.; Misra, S. K.; Ostadhossein, F.; Daza, E.; Singh, J.; Pan, D. Surface Chemistry of Carbon Nanoparticles Functionally Select Their Uptake in Various Stages of Cancer Cells. *Nano Res.* **2017**, *10* (10), 3269–3284. https://doi.org/10.1007/s12274-017-1518-2.
- (4) Liu, M. L.; Chen, B. B.; Li, C. M.; Huang, C. Z. Carbon Dots: Synthesis, Formation Mechanism, Fluorescence Origin and Sensing Applications. *Green Chem.* **2019**, *21* (3), 449–471. https://doi.org/10.1039/C8GC02736F.
- (5) Jiang, K.; Feng, X.; Gao, X.; Wang, Y.; Cai, C.; Li, Z.; Lin, H. Preparation of Multicolor Photoluminescent Carbon Dots by Tuning Surface States. *Nanomaterials (Basel)* **2019**, *9* (4). https://doi.org/10/ggztrg.
- (6) Zhu, S.; Song, Y.; Zhao, X.; Shao, J.; Zhang, J.; Yang, B. The Photoluminescence Mechanism in Carbon Dots (Graphene Quantum Dots, Carbon Nanodots, and Polymer Dots): Current State and Future Perspective. *Nano Res.* **2015**, *8* (2), 355–381. https://doi.org/10.1007/s12274-014-0644-3.
- (7) Nguyen, H. A.; Srivastava, I.; Pan, D.; Gruebele, M. Unraveling the Fluorescence Mechanism of Carbon Dots with Sub-Single-Particle Resolution. *ACS Nano* **2020**, *14* (5), 6127–6137. https://doi.org/10/ggztrq.
- (8) Nguyen, H. A.; Srivastava, I.; Pan, D.; Gruebele, M. Ultrafast Nanometric Imaging of Energy Flow within and between Single Carbon Dots. *Proc Natl Acad Sci USA* **2021**, *118* (11), e2023083118. https://doi.org/10.1073/pnas.2023083118.
- (9) Essner, J. B.; Kist, J. A.; Polo-Parada, L.; Baker, G. A. Artifacts and Errors Associated with the Ubiquitous Presence of Fluorescent Impurities in Carbon Nanodots. *Chem. Mater.* **2018**, *30* (6), 1878–1887. https://doi.org/10.1021/acs.chemmater.7b04446.
- (10) Song, Y.; Zhu, S.; Xiang, S.; Zhao, X.; Zhang, J.; Zhang, H.; Fu, Y.; Yang, B. Investigation into the Fluorescence Quenching Behaviors and Applications of Carbon Dots. *Nanoscale* **2014**, *6* (9), 4676. https://doi.org/10.1039/c4nr00029c.
- (11) Duan, P.; Zhi, B.; Coburn, L.; Haynes, C. L.; Schmidt-Rohr, K. A Molecular Fluorophore in Citric Acid/Ethylenediamine Carbon Dots Identified and Quantified by Multinuclear Solid-state Nuclear Magnetic Resonance. *Magn Reson Chem* **2020**, *58* (11), 1130–1138. https://doi.org/10.1002/mrc.4985.
- (12) Song, Y.; Zhu, S.; Zhang, S.; Fu, Y.; Wang, L.; Zhao, X.; Yang, B. Investigation from Chemical Structure to Photoluminescent Mechanism: A Type of Carbon Dots from the Pyrolysis of Citric Acid and an Amine. *J. Mater. Chem. C* **2015**, *3* (23), 5976–5984. https://doi.org/10.1039/C5TC00813A.
- (13) Jiang, K.; Sun, S.; Zhang, L.; Lu, Y.; Wu, A.; Cai, C.; Lin, H. Red, Green, and Blue Luminescence by Carbon Dots: Full-Color Emission Tuning and Multicolor Cellular Imaging. *Angew. Chem. Int. Ed.* **2015**, *54* (18), 5360–5363. https://doi.org/10.1002/anie.201501193.
- (14) Righetto, M.; Carraro, F.; Privitera, A.; Marafon, G.; Moretto, A.; Ferrante, C. The Elusive Nature of Carbon Nanodot Fluorescence: An Unconventional Perspective. *J. Phys. Chem. C* **2020**, *124* (40), 22314–22320. https://doi.org/10.1021/acs.jpcc.0c06996.
- (15) Qu, D.; Sun, Z. The Formation Mechanism and Fluorophores of Carbon Dots Synthesized *via* a Bottom-up Route. *Mater. Chem. Front.* **2020**, *4* (2), 400–420. https://doi.org/10.1039/C9QM00552H.
- (16) Plachy, T.; Sedlacik, M.; Pavlinek, V.; Morávková, Z.; Hajná, M.; Stejskal, J. An Effect of Carbonization on the Electrorheology of Poly(p-Phenylenediamine). *Carbon* **2013**, *63*, 187–195. https://doi.org/10.1016/j.carbon.2013.06.070.
- (17) Yang, S.; Li, W.; Ye, C.; Wang, G.; Tian, H.; Zhu, C.; He, P.; Ding, G.; Xie, X.; Liu, Y.; Lifshitz, Y.; Lee, S.-T.; Kang, Z.; Jiang, M. C ₃ N-A 2D Crystalline, Hole-Free, Tunable-Narrow-Bandgap Semiconductor with Ferromagnetic Properties. *Adv. Mater.* **2017**, *29* (16), 1605625. https://doi.org/10.1002/adma.201605625.

- (18) Tan, C.; Zhou, C.; Peng, X.; Zhi, H.; Wang, D.; Zhan, Q.; He, S. Sulfuric Acid Assisted Preparation of Red-Emitting Carbonized Polymer Dots and the Application of Bio-Imaging. *Nanoscale Res Lett* **2018**, *13* (1), 272. https://doi.org/10.1186/s11671-018-2657-4.
- (19) Category 2, Hetarenes and Related Ring Systems: Six-Membered Hetarenes with Two Identical Heteroatoms; Yamamoto, Shinkai, Eds.; Georg Thieme Verlag: Stuttgart, 2004; p b-003-121809. https://doi.org/10.1055/b-003-121809.
- (20) Yu, Z.; Park, Y.; Chen, L.; Zhao, B.; Jung, Y. M.; Cong, Q. Preparation of a Superhydrophobic and Peroxidase-like Activity Array Chip for H ₂ O ₂ Sensing by Surface-Enhanced Raman Scattering. *ACS Appl. Mater. Interfaces* **2015**, *7* (42), 23472–23480. https://doi.org/10.1021/acsami.5b08643.
- (21) Matsumura, K. THE FORMATION OF A PHENAZINE COMPOUND FROM A DIPHENYL ETHER DERIVATIVE. *J. Am. Chem. Soc.* **1930**, *52* (8), 3199–3204. https://doi.org/10.1021/ja01371a026.
- (22) Song, S.; Dai, Y.; Hong, Y.; Li, X.; Yan, X. A Simple Continuous Reaction for the Synthesis of Quinoline Compounds. *Green Chem.* **2022**, *24* (4), 1714–1720. https://doi.org/10.1039/D1GC03064G.
- (23) Grimme, S.; Antony, J.; Ehrlich, S.; Krieg, H. A Consistent and Accurate *Ab Initio* Parametrization of Density Functional Dispersion Correction (DFT-D) for the 94 Elements H-Pu. *The Journal of Chemical Physics* **2010**, 132 (15), 154104. https://doi.org/10.1063/1.3382344.
- (24) Yanai, T.; Tew, D. P.; Handy, N. C. A New Hybrid Exchange—Correlation Functional Using the Coulomb-Attenuating Method (CAM-B3LYP). *Chemical Physics Letters* **2004**, *393* (1–3), 51–57. https://doi.org/10.1016/j.cplett.2004.06.011.
- (25) Becke, A. D. Density-functional Thermochemistry. III. The Role of Exact Exchange. *The Journal of Chemical Physics* **1993**, *98* (7), 5648–5652. https://doi.org/10.1063/1.464913.
- (26) Lee, C.; Yang, W.; Parr, R. G. Development of the Colle-Salvetti Correlation-Energy Formula into a Functional of the Electron Density. *Phys. Rev. B* **1988**, *37* (2), 785–789. https://doi.org/10.1103/PhysRevB.37.785.
- (27) Isborn, C. M.; Luehr, N.; Ufimtsev, I. S.; Martínez, T. J. Excited-State Electronic Structure with Configuration Interaction Singles and Tamm–Dancoff Time-Dependent Density Functional Theory on Graphical Processing Units. *J. Chem. Theory Comput.* **2011**, *7* (6), 1814–1823. https://doi.org/10.1021/ct200030k.
- (28) Ufimtsev, I. S.; Martinez, T. J. Quantum Chemistry on Graphical Processing Units. 3. Analytical Energy Gradients, Geometry Optimization, and First Principles Molecular Dynamics. *J. Chem. Theory Comput.* **2009**, *5* (10), 2619–2628. https://doi.org/10.1021/ct9003004.
- (29) Seritan, S.; Bannwarth, C.; Fales, B. S.; Hohenstein, E. G.; Isborn, C. M.; Kokkila-Schumacher, S. I. L.; Li, X.; Liu, F.; Luehr, N.; Snyder, J. W.; Song, C.; Titov, A. V.; Ufimtsev, I. S.; Wang, L.; Martínez, T. J. TERACHEM: A Graphical Processing Unit -ACCELERATED Electronic Structure Package for LARGE-SCALE Ab Initio Molecular Dynamics. WIREs Comput Mol Sci 2021, 11 (2). https://doi.org/10.1002/wcms.1494.
- (30) Humphrey, W.; Dalke, A.; Schulten, K. VMD: Visual Molecular Dynamics. *Journal of Molecular Graphics* **1996**, *14* (1), 33–38. https://doi.org/10.1016/0263-7855(96)00018-5.
- (31) Bartolomei, B.; Bogo, A.; Amato, F.; Ragazzon, G.; Prato, M. Nuclear Magnetic Resonance Reveals Molecular Species in Carbon Nanodot Samples Disclosing Flaws. *Angew Chem Int Ed* **2022**, *61* (20), e202200038. https://doi.org/10.1002/anie.202200038.
- (32) Zhi, B.; Yao, X.; Wu, M.; Mensch, A.; Cui, Y.; Deng, J.; Duchimaza-Heredia, J. J.; Trerayapiwat, K. J.; Niehaus, T.; Nishimoto, Y.; Frank, B. P.; Zhang, Y.; Lewis, R. E.; Kappel, E. A.; Hamers, R. J.; Fairbrother, H. D.; Orr, G.; Murphy, C. J.; Cui, Q.; Haynes, C. L. Multicolor Polymeric Carbon Dots: Synthesis, Separation and Polyamide-Supported Molecular Fluorescence. *Chem. Sci.* **2021**, *12* (7), 2441–2455. https://doi.org/10.1039/D0SC05743F.